Low energy, ion-induced electron and ion emission from stainless steel: The effect of oxygen coverage and the implications for discharge modeling

S. G. Walton, J. C. Tucek,[a] and R. L. Champion
Department of Physics, College of William and Mary, Williamsburg, Virginia 23187

Yicheng Wang[b]
National Institute of Standards and Technology, Gaithersburg, Maryland 20899

(Received 23 July 1998; accepted for publication 26 October 1998)

Absolute yields of electrons and negative ions resulting from positive ions impacting stainless steel have been determined as a function of impact energy for clean and oxygen-covered surfaces. Photoelectron emission has been used to monitor the effect of oxygen coverage on the surface work function. The emission of negative ions and electrons has been described with an excitation mechanism similar to that used in the Menzel–Gomer–Redhead model. We illustrate the implications of the present observations for discharge modeling and diagnostics by citing a parallel-plate, rf discharge in oxygen as an example. © *1999 American Institute of Physics.* [S0021-8979(99)05503-6]

I. INTRODUCTION

Plasma discharges are widely used to modify the surface properties of materials. By controlling plasma-surface interactions, effects such as differential etching, thin film deposition, or surface cleaning may be achieved. Substantial effort has been directed toward optimizing and understanding the processes responsible for the surface modifications. Plasma-surface interactions also influence the bulk discharge, notably through emission of electrons and negative secondary ions from the surface due to positive ion bombardment. In some cases, a secondary process can control the discharge properties. For example, in a capacitively coupled rf discharge, electrons resulting from ion bombardment of electrodes are accelerated through the sheath potential into the bulk of the plasma. As the discharge voltage increases, ionization due to such electrons can become dominant and lead to the so-called $\alpha \rightarrow \gamma$ mode transition. These two modes differ dramatically in light emission and electron energy distributions.[1]

A knowledge of the processes induced by positive ion impact is crucial in understanding and ultimately controlling plasma reactions. Recent studies of electron and negative secondary ion emission from well characterized elemental metallic surfaces[2,3] have illustrated that electron and negative ion yields dramatically increase with increasing oxygen coverage for impact energies common to discharge environments, viz, in the region of a few hundred eV. Results for ion-induced emission of electrons and anions from a "technical" stainless steel surface, i.e., one which has *not* been cleaned under ultrahigh vacuum (UHV) conditions, have been communicated previously.[4] In that study, it was found that the anion yield could be as large as 0.1 and exceed the electron yield for a large range of impact energies. For the technical surface, the secondary anions were predominately O^- and O_2^-. That observation may have significant implications in interpreting some recent theoretical and experimental results reported in this journal: recent model simulations of capacitively coupled, rf oxygen discharges by Shibata *et al.*[5] predicted the O^- density to exceed that for O_2^- by several orders of magnitude. In fact, however, O^- and O_2^- concentrations were observed by Zeuner *et al.*[6] to be comparable in rf plasmas under conditions similar to those used for the simulation. This discrepancy may be due to the fact that secondary negative ion emission was omitted in the simulations and the experimental arrangement preferentially detected the more energetic negative ions originating from the electrode surfaces.

The aim of the present work is twofold. The first is to investigate the role of adsorbed oxygen in ion-induced electron and negative ion emission from clean and oxygen-covered 302 stainless steel surfaces which have been exposed to a small and controlled amount of oxygen, and to describe that emission in terms of a model used previously for emission from other oxygen-covered surfaces.[3,7] As a reference, the results for stainless steel will be compared to those for polycrystalline Al,[2,7] another commonly used electrode metal. We will then indicate how the observations may be used to interpret and compare the experimental and theoretical results for the O_2 discharges cited above.

II. EXPERIMENTAL METHOD

The experimental apparatus has been described in detail elsewhere.[2,7] Briefly, the experiments are conducted in a UHV chamber with a base pressure $<2\times10^{-10}$ Torr. The metal sample used is 302 stainless steel ribbon. The primary Na^+ beam is provided by an ion gun aligned at 60° with respect to the surface normal. Sodium was chosen for the

[a]Present address: Argonne National Laboratory, Materials Science and Chemistry Division, Argonne, IL 60439.
[b]Electronic mail: wang@eeel.nist.gov

impacting ion to eliminate the possibility of potential emission of electrons as the ionization potential (~5 eV) is less than twice the work function of stainless steel, the minimum required for potential emission.[8] The impact energies range up to 500 eV, an energy range for which the probability of kinetic emission of electrons is very small.[9] All negatively charged products ejected from the surface are focused along the surface normal by a series of electrostatic lenses. A majority of the negative products (~70%) is collected on the lens closest to the surface. The remaining products are focused for further analysis and a small electromagnet may be used to remove the electrons from the extracted products, thus enabling independent measurements of the electron and anion yields. It is assumed that the ratio of electrons to anions in the sampled portion of the focused beam is an accurate reflection of that for all negative products. This assumption is supported by the observation that the measured ratio does not depend upon focal conditions for a wide range of focusing voltages. The estimated uncertainty for the yield measurements is 10%. The kinetic energy distributions are measured with a double spherical electrostatic energy analyzer with a resolution, $\Delta E/E$, of 0.008. Diagnostic measurements include time-of-flight secondary ion mass spectroscopy (TOF-SIMS) and Auger electron spectroscopy (AES).

The surface was cleaned by two consecutive cycles of sputtering and annealing. The sputtering was achieved by rastering a 3.5 KeV, 1 μA Ar^+ beam across the surface for 45 min and then annealing by 15 min of resistive heating to >600 °C. SIMS and AES measurements were employed to confirm that no adsorbates were present on the surface after cleaning. Exposure of the surface to oxygen was accomplished with a precision leak valve and measured by a residual gas analyzer. For the present work, exposure is expressed in terms of Langmuir (L), where $1\ L = 10^{-6}$ Torr s. Since the presence of alkali metal has been shown to lower the surface work function and increase negative ion emission,[10,11] great care was taken to limit the Na^+ dose during the experiments. TOF-SIMS analyses taken after the yield and kinetic energy distribution measurements confirmed a negligible Na accumulation.

Photoelectron emission has been used to ascertain the work function of clean stainless steel and the effect of oxygen coverage on the work function. These measurements were conducted at the Synchrotron Radiation Center operated by the University of Wisconsin-Madison. The beamline (SS SEYA) allows for low energy photoemission measurements under UHV conditions with a base pressure of $\sim 2 \times 10^{-10}$ Torr. The measurements reported here were made using 23.0 eV photons selected by a Seya–Namikoa[12] monochrometer with a linear dispersion of 8.33 Å/mm. With entrance and exit slit widths of 300 μm, the uncertainty in photon energy was ±5 meV. The associated kinetic energy distributions for angle integrated photoelectrons were made using a double-pass, cylindrical mirror analyzer. With a pass energy of 5 eV, the resolution of the analyzer was better than 0.16 eV which, given the small uncertainty in photon energy, is the effective resolution for the electron spectra. All electron kinetic energy distributions are normalized to the photoelectric current produced by a 90% transmitting Ni mesh located after the monochrometer.

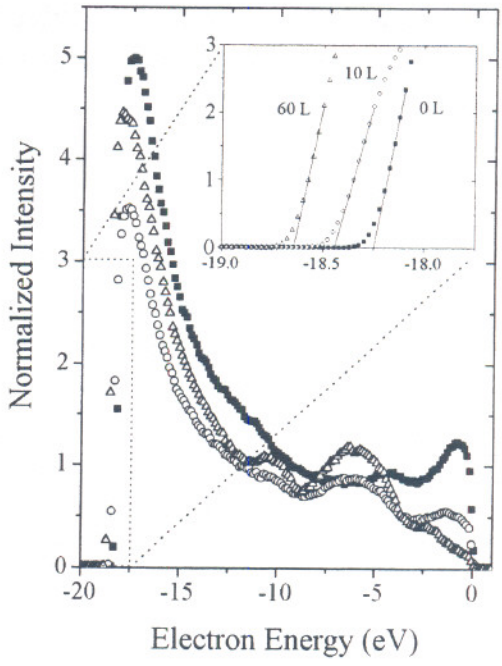

FIG. 1. Photoelectron spectra for a stainless steel surface are shown for a clean surface (■) and surfaces exposed to 10 L (○) and 60 L (△) of oxygen. The inset clearly illustrates the change (decrease) in the work function as oxygen accumulates on the surface. The zero of the energy scale refers to a photoelectron from the top of the conduction band.

III. RESULTS

A. Photoemission

Industry standards hold that 302 stainless steel be comprised of 68%–72% Fe, 17%–19% Cr, and 8%–10% Ni with trace amounts of C, Mn, P, S, and Si. Oxygen adsorption sites and the surface work function will depend on the surface structure which, for stainless steel, is not homogeneous. Nevertheless, it is possible to determine an average oxygen uptake and work function, Φ. Photoelectron spectra are exhibited in Fig. 1 for clean and oxygen-covered surfaces. The energy scale in Fig. 1 represents $E' = E + \Phi - E_{h\nu}$, where E is the kinetic energy of an ejected photoelectron and $E_{h\nu}$ is the photon energy, which is 23.0 eV. The zero for E' is thus defined for the *most* energetic photoelectrons, i.e., those which originate from the Fermi edge. The work function is then obtained by setting E to zero

$$\Phi = E_{h\nu} + E_0', \tag{1}$$

where the onset of photoemission, E_0', is determined by a linear extrapolation of the photoelectron intensity to zero.[13,14] Such extrapolations are seen in the inset in Fig. 1, where for a clean surface, $E_0' = -18.25$ eV, yielding Φ (clean) = 4.75 eV. As can be seen in the inset of Fig. 1, the work function decreases by 0.2 and 0.4 eV for oxygen exposures of 10 and 60 L, respectively.

The spectra in Fig. 1 also clearly demonstrate the effect of oxygen on the density of states near the Fermi edge. In good agreement with ultraviolet photoelectron spectroscopy

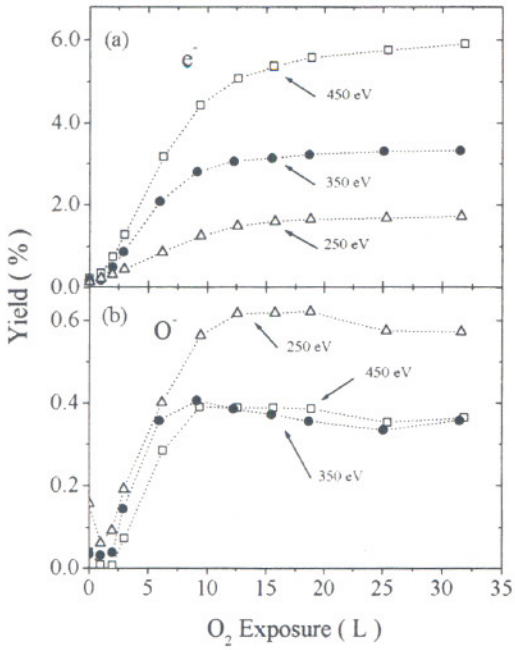

FIG. 2. (a) Absolute electron yields for Na^+ impacting stainless steel at 250 eV (△), 350 eV (●), and 450 eV (□) as a function of oxygen exposure. (b) Absolute O^- yields for the same Na^+ impact energies.

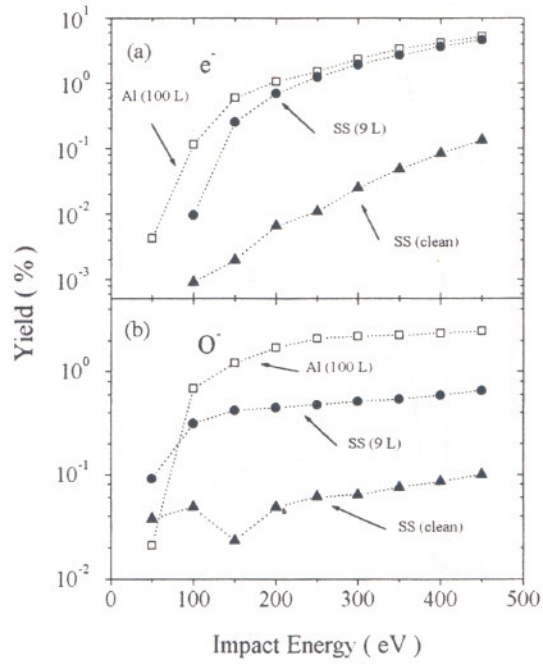

FIG. 3. (a) A comparison of the absolute electron yields for aluminum and stainless steel as a result of Na^+ impact. The (□) are for an Al substrate exposed to 100 L of oxygen, while (▲) are the results for clean stainless steel surface and (●) for an exposure of 9 L. (b) A comparison of O^- yields for the same conditions.

(UPS) studies of oxygen chemisorption on metals,[15–17] the appearance of an oxygen-induced state at 6–7 eV below the Fermi level is apparent and is typically attributed to the $2p$ level of the adsorbed oxygen. An accompanying decrease in the density of states near the Fermi level is indicative of a charge transfer between the substrate and the adsorbed oxygen. This charge transfer has been shown to result in additional charge around the oxygen, making it ionic in nature.[18]

B. Ion-induced emission of electrons and anions

TOF-SIMS shows that O^- is the dominant secondary ion for exposures up to 100 L of oxygen, comprising ~90% of the spectrum for oxygen-adsorbed stainless steel surfaces. As expected, higher mass products such as FeO^- and CrO^- are also observed, but owing to poor resolution at higher mass, they cannot be identified unambiguously. The ion-induced electron yields (Y_e) and the anion yields (Y_0^-) as a function of exposure for three impact energies are given in Figs. 2(a) and 2(b), respectively. The electron yield clearly increases with energy and the amount of adsorbed oxygen and appears to saturate for exposures of 10–15 L. The ion yield exhibits a minimum for an exposure of about 2 L and increases thereafter, saturating at 10 L. Note that annealing (which is done immediately before the yield measurements) can cause C, Mn, and S to migrate to the surface[13,19] and these trace elements may combine with oxygen to form volatile compounds such as CO and SO_2 which subsequently desorb from the surface. Until the surface is free of these contaminates, the chemisorption of oxygen on the substrate will not occur. The results of Fig. 2(b) suggest that such a "surface cleaning" may occur for an oxygen exposure of 2 L. The observed saturation of O^- emission at 10 L is in good agreement with the results of Blasek and Weihert,[20] who use the emission of O^- to suggest that the formation of one monolayer (ML) occurs at 6–7 L.

In Fig. 3 the yields are given as a function of impact energy for a clean surface and one with about 1 ML of adsorbed oxygen. It is apparent that the presence of oxygen on the surface greatly enhances electron and secondary anion emission, particularly at higher impact energies where the increase in Y_{0^-} is sixfold and the increase in Y_e is in excess of an order of magnitude. A comparison with aluminum is also shown in Fig. 3 for coverage of about 1 ML. Generally, the electron yields and their enhancements are similar for the two substrates while the sputtering of O^- is significant for stainless steel but not as large as that observed for Al.

C. Kinetic energy distributions

Anion and electron kinetic energy distributions are shown in Fig. 4 for an exposure of 12 L. The O^- distributions exhibit a high energy, low level tail with a most probable energy at 1.5 eV. The electron spectra exhibit a similar peak at 1.5 eV and a full width at half maximum (FWHM) of 1.7 eV with a small high energy tail. These distributions are found to be essentially independent of both oxygen exposure and impact energy and are very similar to those observed for Al.[7] In comparison with stainless steel, the spectra from Al exhibit slightly smaller mean energies (~1 eV) and the electron energy distributions show slightly smaller widths (1.0–1.5 eV).

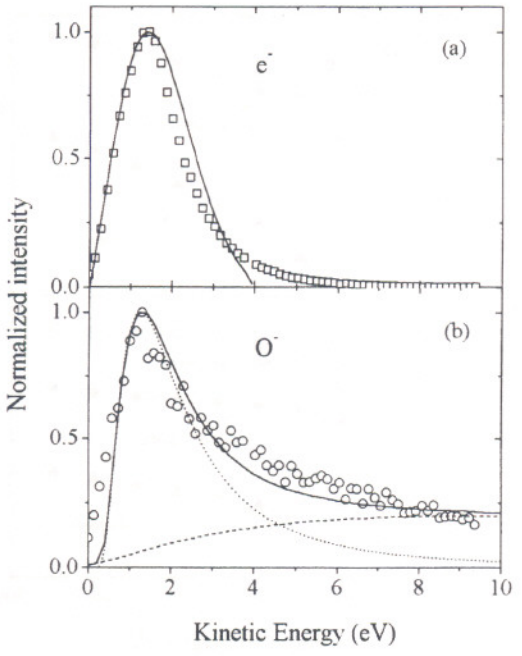

FIG. 4. (a) The electron kinetic energy distributions for a 12 L oxygen exposed stainless steel surface at an impact energy of 450 eV. The solid line is the distribution predicted by the excitation mechanism. (b) The O^- kinetic energy distribution for the same conditions. The dotted line is the distribution predicted by the excitation mechanism and the dashed line is the distribution predicted by the modified collision cascade. The solid line represents the sum of the two distributions.

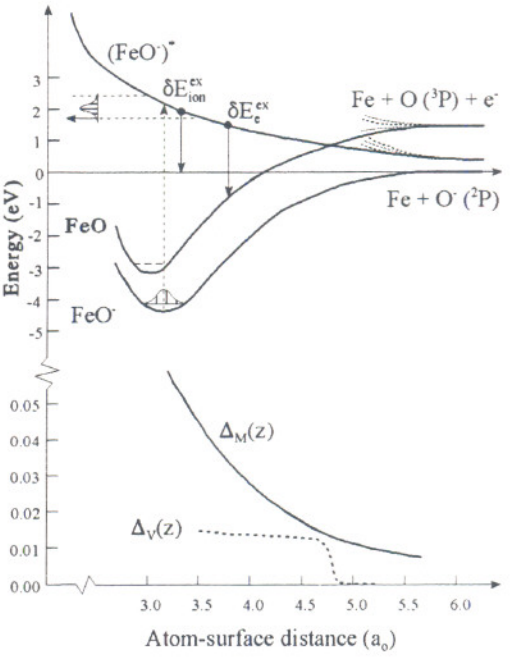

FIG. 5. Schematic diagram of the molecular states for the interaction of O and O^- with Fe as a function of distance from the surface. Also shown are the decay widths used to describe the two electron decay channels. The FeO and FeO^- ground states are representative of isolated molecular curves.

IV. DISCUSSION

A. Model for secondary emission

The present results for ion-induced electron emission cannot be described in terms of either conventional potential[8] or kinetic[9] emission models as the ionization potential of Na is too small for the former and the impact energy is too low for the latter. In an attempt to explain similar emission observed for other oxygen-metal systems,[3,7] a model was proposed which invoked a collision-induced electronic transition of a surface state which subsequently led to either electron or anion emission. In many respects that model is similar to the Menzel–Gomer–Redhead[21,22] theory used to describe electron-induced ion emission. We will extend the model, the details of which may be found in Refs. 3 and 7, to discuss the observations for stainless steel.

Let us assume that oxygen dissociatively chemisorbs on stainless steel,[13,20] and thus oxygen resides on the surface essentially as a negative ion. For illustrative purposes, we will assume the formation of FeO^-, shown in Fig. 5, at an equilibrium distance from the surface, $Z_{eq} \approx 3$ Å. The idea is that an impacting ion (or atom) electronically excites FeO^- to an antibonding state, $(FeO^-)^*$. After excitation, the negative ion can exit the surface and survive, or decay by electron emission either to the metal [with width $\Delta_m(z)$] or to the vacuum [with width $\Delta_v(z)$]. Electron emission to the vacuum can occur at any distance where the energy of the $(FeO^-)^*$ lies above that for FeO, while emission to the metal can occur for any distance. The latter decay channel is, by far, the dominant channel. The kinetic energy of the electron emitted to the vacuum is represented by the difference, δE_e. In the case where the ion exits the surface and survives as a negative ion, its kinetic energy is represented by the difference δE_{ion}. An additional mechanism which may give rise to O^- emission involves momentum transfer from the impacting Na^+ directly to the adsorbed oxygen or indirectly through collisions with the substrate atoms. Such ejection processes for neutral atoms have been described with the so-called "collision cascade" model.[23,24] In previous work,[3,7] that model was modified to account for the survival probability of the negative ion as it departs the surface.[25,26] The anion kinetic energy distribution that arises from such a modified collision cascade model is quite different from that found for neutral atoms. In particular, the survival probability for low energy ions is quite small, resulting in a very broad energy distribution which in no way resembles what is observed in, e.g., Fig. 4.

The diagram in Fig. 5 is based partly on gas-phase intermolecular potentials for FeO and FeO^- and can only provide an estimate of the ion-surface interactions, since the surface is undoubtably more complicated. The width for electron decay into the metal, $\Delta_m(z)$, is similar to that calculated for the Al/O^- surface interaction.[27] The remaining parameters are adjusted to bring the calculation into agreement with the observed energy distributions. Several features in a similar *ad hoc* diagram designed to explain ion-induced electron emission from an Al/O surface have been confirmed with studies involving photon-induced anion emission.[28] Much like the diagrams which describe the Menzel–Gomer–Redhead[21,22] theory of electron-induced ion emission, this diagram is used to demonstrate a mechanism that can, using reasonable parameters, account for electron emission and reproduce the observed kinetic energy distributions.

Calculated electron and anion distributions based on the potential parameters shown in Fig. 5 are given in Figs. 4(a) and 4(b), respectively. For the ion distribution, the result of the excitation mechanism is added to that predicted by the aforementioned modified collision cascade model to provide a good fit to the experimental observations: the excitation mechanism is responsible for about 2/3 of the secondary anions and provides the low energy peak while the collision cascade provides the high energy tail.

B. Implications for discharge modeling and diagnostics

The present results for ion-induced emission of electrons and secondary ions from a stainless steel surface clearly show that the yield of both anions and electrons can be quite large and depends very strongly on the ion impact energy and the surface conditions. In contrast to the well-recognized importance of electron emission, negative ion emission is neglected in the description of discharges. If anion and electron emission from electrodes are comparable, as can be the case for stainless steel electrodes in discharge environments,[4] such an omission may compromise the accuracy of discharge simulations and diagnostic interpretations. Let us take a parallel-plate, rf discharge in oxygen as an example. Recent model simulations by Shibata *et al.*[5] for capacitively coupled rf discharges in 0.5 Torr oxygen at 13.6 MHZ and 150 V rf voltage indicate that the negative ion density approaches that for positive ions in the bulk plasma, with electrons comprising only a small fraction of the total negative charge. The dominant negative ion species is predicted to be O^- with O_2^- forming only about 2%–3% of the total negative ion density. Their results also indicate that electron attachment occurs mainly in the bulk plasma and the negative ions formed are largely trapped by the plasma sheath potentials. Consequently, the ratio of anions to cations, which traverse the sheath and arrive at the electrode surface, is predicted to be less than 10^{-5}. On the other hand, experimental observations by Zeuner *et al.*[6] in rf plasmas operating with conditions similar to those described above show some seemingly contradictory results. First, the anion to cation ratio at the ground electrode increases with increasing rf voltage and is significantly higher than the prediction, ranging from 0.01 to 0.1. Secondly, the O_2^- and O^- ion fluxes are found to be comparable and have kinetic energies as high as the self-bias voltage of the powered electrode. This behavior of the negative ions was attributed to electron attachment occurring in the sheath near the powered electrode.[6]

We suggest an alternative explanation for the reported large negative ion flux, viz., the observed negative ions were secondary ions emitted from the powered electrode due to impacting positive ions, predominantly O_2^+ in oxygen discharges. The dominant negative ion production mechanism in the bulk of an oxygen discharge is dissociative attachment, forming O^-. While O_2^- can form indirectly by electron transfer, $O^- + O_2 \rightarrow O + O_2^-$, this process has an energetic threshold of about 1 eV, resulting in a very slow O_2^- formation rate in a low temperature plasma. The negative ions that are formed in the bulk plasma will be trapped by the sheath potentials, but the secondary negative ions O^- and O_2^- emitted from the powered electrode will have sufficient energy to penetrate the bulk plasma and overcome the sheath potential barrier near the ground electrode. While traversing the electrode gap, O^- may be destroyed by electron transfer or electron detachment in collisions with O_2. Taking a combined cross section of 8 $Å^2$ for these two processes,[29] an electrode separation of 3 cm and gas pressure of 1.5 Pa, as used by Zeuner *et al.*, the probability that O^-, produced on the powered electrode, reaches the ground electrode intact can be estimated to be 0.38. The behavior of O_2^- in traversing the sheath is more complicated because of the large electron transfer cross section for low collision energies in the O_2 parent gas. Under any circumstances, the sheath potential of the powered electrode is significantly higher than that of the ground electrode,[30] and thus the majority of slow O_2^- ions formed in the powered sheath will again be accelerated to energies high enough to overcome the potential of the ground sheath. If we consider only the loss of fast O_2^- in the bulk plasma and take the combined cross section for electron transfer and electron detachment to be 14 $Å^2$ at 200 eV,[29] the probability that a fast O_2^- ion will reach the ground electrode can be estimated to be 0.19. Hence, if the emission probabilities of O_2^- and O^- are similar at the powered electrode (as is the case when surface conditions approximate those found in discharge environments[4]), comparable intensities of atomic and molecular anions would reach the grounded electrode, a feature that has been observed[6] for the oxygen rf discharge.

V. CONCLUSIONS

It is clear that the probabilities for ion-induced emission of electrons and negative ions from stainless steel depend strongly on the surface conditions, ranging from negligibly small for a sputtered-clean surface to as high as 0.1 for a technical surface, i.e., one which has not been cleaned *in situ* under UHV conditions. For clean surfaces which have been exposed to a moderate amount of oxygen, the dominant secondary negative ion is O^-. For the technical surface, however, secondary O^- and O_2^- ions are comparable in number. The present study demonstrates that if we wish to correctly model an oxygen discharge, an understanding of the electron and ion emissions is required not only for a well characterized surface, but also for a surface that mimics the actual electrode surface immersed in a plasma.

ACKNOWLEDGMENTS

This work was supported by the U.S. Department of Energy, Office of Basic Energy Sciences, Division of Chemical Sciences. The photoemission studies were performed at the SRC, University of Wisconsin-Madison, which is supported by the NSF under Award No. DMR-95-31009.

[1] V. A. Godyak, R. B. Piejak, and B. M. Alexandrovich, Phys. Rev. Lett. **68**, 40 (1992).
[2] J. C. Tucek, S. G. Walton, and R. L. Champion, Phys. Rev. B **53**, 14127 (1996).
[3] J. C. Tucek, S. G. Walton, and R. L. Champion, Surf. Sci. **410**, 258 (1998).

[4] S. G. Walton, R. L. Champion, and Y. Wang, J. Appl. Phys. **84**, 1706 (1998).
[5] M. Shibata, N. Nakano, and T. Makabe, J. Appl. Phys. **77**, 6181 (1995).
[6] M. Zeuner, J. Meichsner, and J. A. Rees, J. Appl. Phys. **79**, 9379 (1996).
[7] J. C. Tucek and R. L. Champion, Surf. Sci. **382**, 137 (1997).
[8] H. D. Hagstrum, Phys. Rev. **96**, 336 (1955).
[9] E. V. Alonso, M. A. Alurralde, and R. A. Baragiola, Surf. Sci. **166**, L155 (1986).
[10] M. L. Yu, Phys. Rev. Lett. **40**, 574 (1978); Phys. Rev. B **26**, 4731 (1982).
[11] M. Bernhiem and F. LeBourse, Nucl. Instrum. Methods Phys. Res. B **27**, 94 (1987).
[12] T. Namioka, M. Seya, and H. Noda, Jpn. J. Appl. Phys. **15**, 1181 (1976).
[13] C. Jardin, B. M. Duc, J. P. Gauthier, G. Thollet, and P. Michel, J. Electron Spectrosc. Relat. Phenom. **19**, 213 (1980).
[14] S. Evans, Chem. Phys. Lett. **23**, 134 (1973).
[15] K. Y. Yu, W. E. Spicer, I. Lindau, P. Pianetta, and S. F. Lin, Surf. Sci. **57**, 157 (1976).
[16] T. Komeda, Y. Sakisaka, and M. Onchi, Phys. Rev. B **38**, 7345 (1988).
[17] K. Y. Yu, J. N. Miller, P. Chye, W. E. Spicer, N. D. Lang, and A. R. Williams, Phys. Rev. B **14**, 1446 (1976).
[18] D. S. Wang, A. J. Freeman, and H. Krakauer, Phys. Rev. B **24**, 3092 (1981).
[19] R. K. Wild, in Proceedings of the Conference on the Interactions of Electrons with Solids, Vacuum **26**, 441 (1976), and the references therein.
[20] G. Blasek and M. Weihert, Surf. Sci. **82**, 215 (1979).
[21] D. Menzel and R. Gomer, J. Chem. Phys. **41**, 3311 (1964).
[22] P. A. Redhead, Can. J. Phys. **42**, 886 (1964).
[23] M. W. Thompson, Philos. Mag. **18**, 377 (1968).
[24] P. Sigmund, in *Sputtering by Particle Bombardment I*, edited by R. Behrisch (Springer, Berlin, 1981), pp. 9–72.
[25] N. D. Lang and J. K. Nørskov, Phys. Scr. **6**, 15 (1983).
[26] M. L. Yu and N. D. Lang, Nucl. Instrum. Methods Phys. Res. B **14**, 403 (1986).
[27] B. Bahrim, D. Teillet-Billy, and J. P. Gauyacq, Phys. Rev. B **50**, 7860 (1994); Surf. Sci. **316**, 189 (1994).
[28] S. G. Walton, B. L. Peko, and R. L. Champion, Phys. Rev. B **58**, 15430 (1998).
[29] T. L. Bailey and P. Mahadevan, J. Chem. Phys. **52**, 179 (1970).
[30] Y. Wang, Appl. Phys. Lett. **66**, 2186 (1995).